Experimental Neurology 267 (2015) 143–151

Contents lists available at ScienceDirect

Experimental Neurology

journal homepage: www.elsevier.com/locate/yexnr

Regular Article

ENU mutagenesis identifies mice modeling Warburg Micro Syndrome with sensory axon degeneration caused by a deletion in *Rab18*

Chih-Ya Cheng [a], Jaw-Ching Wu [a,b,c], Jin-Wu Tsai [d,e], Fang-Shin Nian [d], Pei-Chun Wu [e,f], Lung-Sen Kao [e,f], Ming-Ji Fann [e,f], Shih-Jen Tsai [g,h], Ying-Jay Liou [g,h], Chin-Yin Tai [i], Chen-Jee Hong [d,g,h,*]

[a] Institute of Clinical Medicine, National Yang-Ming University, Taipei, Taiwan
[b] Institute of Clinical Medicine and Cancer Research Center, National Yang-Ming University, Taipei, Taiwan
[c] Department of Medical Research and Education, Taipei Veterans General Hospital, Taipei, Taiwan
[d] Institute of Brain Science, National Yang-Ming University, Taipei, Taiwan
[e] Brain Research Center, National Yang-Ming University, Taipei, Taiwan
[f] Department of Life Sciences and Institute of Genome Sciences, National Yang-Ming University, Taipei, Taiwan
[g] Division of Psychiatry, School of Medicine, National Yang-Ming University, Taipei, Taiwan
[h] Department of Psychiatry, Taipei Veterans General Hospital, Taipei, Taiwan
[i] Institute of Molecular Biology, Academia Sinica, Nankang, Taipei, Taiwan

ARTICLE INFO

Article history:
Received 21 December 2014
Accepted 5 March 2015
Available online 13 March 2015

Keywords:
Rab18
Warburg Micro Syndrome
Axonal degeneration
Sensory
Stomping gait

ABSTRACT

Mutations in the gene of *RAB18*, a member of Ras superfamily of small G-proteins, cause Warburg Micro Syndrome (WARBM) which is characterized by defective neurodevelopmental and ophthalmological phenotypes. Despite loss of Rab18 had been reported to induce disruption of the endoplasmic reticulum structure and neuronal cytoskeleton organization, parts of the pathogenic mechanism caused by *RAB18* mutation remain unclear. From the *N*-ethyl-*N*-nitrosourea (ENU)-induced mutagenesis library, we identified a mouse line whose *Rab18* was knocked out. This $Rab18^{-/-}$ mouse exhibited stomping gait, smaller testis and eyes, mimicking several features of WARBM. $Rab18^{-/-}$ mice were obviously less sensitive to pain and touch than WT mice. Histological examinations on $Rab18^{-/-}$ mice revealed progressive axonal degeneration in the optic nerves, dorsal column of the spinal cord and sensory roots of the spinal nerves while the motor roots were spared. All the behavioral and pathological changes that resulted from abnormalities in the sensory axons were prevented by introducing an extra copy of *Rab18* transgene in $Rab18^{-/-}$ mice. Our results reveal that sensory axonal degeneration is the primary cause of stomping gait and progressive weakness of the hind limbs in $Rab18^{-/-}$ mice, and optic nerve degeneration should be the major pathology of progressive optic atrophy in children with WARBM. Our results indicate that the sensory nervous system is more vulnerable to Rab18 deficiency and WARBM is not only a neurodevelopmental but also neurodegenerative disease.

Introduction

Warburg Micro Syndrome (WARBM) is an autosomal recessive disorder that presents with ocular and neurological symptoms (Abdel-Salam et al., 2007; Derbent et al., 2004; Handley et al., 2013; Warburg et al., 1993). Affected patients have severe vision impairment, including congenital cataracts, small atonic pupils, microcornea, microphthalmia and progressive visual loss. Neurological phenotypes include postnatal microcephaly, profound mental retardation, congenital hypotonia, epilepsy, and progressive limb spasticity. Although they were born with normal head circumferences, their head circumferences fell to between 4SD and 6SD below the mean at age 12 months (Bem et al., 2011). Brain MRI studies further showed structural defects in the nervous system, including bilateral polymicrogyria, hypogenesis of the corpus callosum and cerebellar vermis hypoplasia. These patients also display impairments in the reproductive system with characteristic microgenitalia in males that may result in infertility (Aligianis et al., 2005). Although the clinical features of WARBM patients with progressive visual loss and progressive limb spasticity, WARBM is usually regarded as a developmental disorder of the nervous system. Knockdown of *rab18* in zebrafish exhibiting a general developmental delay also suggested a conserved developmental role with *rab18* (Bem et al., 2011). Using a number of genetic analyses, mutations in four genes have been found so far: *RAB3GAP1*, *RAB3GAP2*, *RAB18* and *TBC1D20* (Bem et al., 2011; Aligianis et al., 2005; Borck et al., 2011; Liegel et al., 2013).

The Rab family is part of Ras-related, small GTPase proteins, which are central regulators of vesicle budding, tethering, and fusion. Rabs

* Corresponding author at: Department of Psychiatry, Taipei Veterans General Hospital, Taipei, Taiwan.
E-mail address: cjhong007@gmail.com (C.-J. Hong).

http://dx.doi.org/10.1016/j.expneurol.2015.03.003
0014-4886/

act as molecular switches, cycling between 'inactive' GDP-bound and 'active' GTP-bound states. Conversion from the GDP- to the GTP-bound form is catalyzed by a GDP/GTP exchange factor (GEF). Conversion from the GTP- to the GDP-bound form is stimulated by a GTPase-activating protein (GAP) (Stenmark and Olkkonen, 2001; Takai et al., 2001; Corbeel and Freson, 2008; Goody et al., 2005). Distinct Rabs are activated by a specific GAPs and GEFs. TBC1D20 has been established as a GAP for Rab1 and Rab2, which is implicated in the regulation of the traffic between COPII dependent ER and the Golgi complex (Liegel et al., 2013; Haas et al., 2007; Sklan et al., 2007). The RAB3GAP complex has specific GAP activity for the RAB3 family, regulating synaptic transmission and plasticity (Sakane et al., 2006) and specific GEF activity for RAB18, regulating endoplasmic reticulum (ER) morphology (Gerondopoulos et al., 2014). In the absence of either Rab3GAP subunit or Rab18 function, ER tubular networks were disrupted, and ER sheets spread out into the cell periphery (Gerondopoulos et al., 2014).

To investigate the molecular mechanism of WARBM, mouse models of *Rab3GAP1* and *TBC1D20* have been built. Loss of the *Rab3gap1* gene in mice did not show any ocular and neurodevelopmental defects (Sakane et al., 2006). Another mouse model, the *blind sterile* (*bs*) mouse, contains a spontaneous loss-of-function mutation in *TBC1D20*. The *bs* mice exhibit embryonic cataracts and spermatid abnormalities, however, did not show other severe behavioral phenotypes found in human patients (Liegel et al., 2013). More recently, a *Rab18* knockout mouse exhibiting congenital nuclear cataracts, atonic pupils and progressive weakness of the hind limbs was reported to show accumulations of neurofilament in synaptic terminals and cytoskeletal disorganization in the sciatic nerve (Carpanini et al., 2014). However, widespread disruption of neuronal cytoskeleton cannot clearly explain the severity of the gait problem in $Rab18^{-/-}$ mice.

In the present study, we identified a mouse line with a *Rab18*-null mutation from a mouse mutant library obtained by ENU-induced mutagenesis. Homozygotes of *Rab18*-null alleles ($Rab18^{-/-}$) exhibited stomping gait, microphthalmia and microgenitalia similar to the clinical symptoms of patient with WARBM. We found that loss of Rab18 selectively caused sensory axonal degeneration which resulted in sensory ataxia and impaired perceptions to pain and touch. The sensory pathology has never been reported and could be the major pathology of progressive visual loss and progressive limb spasticity in patients with WARBM. Our results indicate that the sensory nervous system is more vulnerable to Rab18 deficiency and WARBM is not simply a developmental disease but also a neurodegenerative disease.

Materials and methods

Generation of ENU-mutagenized mice

Mutagenized mice were produced in the Mouse Mutagenesis Program Core Facility (MMPCF), Academia Sinica, Taiwan. C57BL/6J male mice were administered three injections of *N*-ethyl-*N*-nitrosourea (ENU) (i.p., 100 mg/kg body weight; Sigma) to generate G0 mice. ENU-treated mice were bred according to the three-generation breeding scheme (Fig. S1) as described by Weber et al. (2000). G3 offspring were used for recessive phenotypic screens (Justice, 2000; Balling, 2001; Hrabe de Angelis et al., 2000). After proving heritability of the stomping phenotype, all mice were conveyed to the animal room of Taipei Veterans General Hospital for further experiments. All experiments were approved by Academia Sinica and Taipei Veterans General Hospital, Taiwan for animal care and use.

Gene mapping

Mapping of the mutation was performed using a standard outcross strategy to BALB/c mice in combination with SNP markers specific for the C57BL/6J and BALB/c strains. Eight stomping F2 mice were selected for initial mapping in which 40 probes were used for analysis (Neuhaus and Beier, 1998). To further narrow the interval, primers and probes flanking the SNPs in chromosome 18 were designed in two stages in multiplex format using SpectroDESIGNER software (Sequenom, San Diego, CA). SNP genotyping was performed using high-throughput MALDI-TOF mass spectrometry (Jurinke et al., 2002). Gene mapping analysis was conducted by constructing and comparing figures, as shown in Fig. S2. Mutation detection within the nonrecombinant region was sequenced using a BigDye dideoxy-terminator system and analyzed on an ABI 3700 sequencer (Applied Biosystems, Foster City, CA).

Endogenous Rab18 genotyping

The primers used were Rab18-f13: 5′-GACAAAGTCAACAGGCAA-3′, Rab18-f14: 5′-ACAAATGCCTGCATACAG-3′ and Rab18-b12: 5′-CTCTAT ACTTGGGTCATC-3′. The deleted allele was presented as a 417 bp PCR product amplified with f13 and b12 primers, while a normal allele (without deletion) was presented as a 463 bp PCR product amplified with f14 and b12 primers.

Tail suspension photography

Mice were suspended by attaching their tails with adhesive tape to the border of a desk. Mice usually struggled for 2–3 min then attained a posture of immobility which was photographed.

Genetic rescue

Rab18 cDNA obtained from the cerebellum of a WT C57BL/6 mouse was amplified with forward primer: 5′-CCGGAATTCACGGGGGCTGGGT CGGAGTAGAGCGG GCGCACCATGGACGAGGACGTGCTGA-3′ and backward primer: 5′-CGCGGAT CCGCGTTATAGCACAGAGCAGTAACCGCCG CAGGCGCCTCCTCCTCTGCT CTCTTCC-3′. The poly(A) signal was amplified from pIRES-EGFP (Clontech) with primers: 5′-GGACTAGTCTGTAC AAGTAAAGCGGC-3′ and 5′-TGCTCTAGAG CAGTTTGGACAAACCACAAC-3′. The PCR primers used to identify the transgene were HS4-F: 5′-CCTCCTTGGGCAACCTGTTCAG-3′ and HS4-R: 5′-ATGTGGCA CTGAGG GACATGGC-3′.

Western blot analysis

The cerebellum were rinsed in PBS and homogenized in chilled NP-40 lysis buffer containing a protease inhibitor cocktail (Sigma, St. Louis). Lysates were clarified by centrifugation. Protein concentrations were determined using the Lowry method and BSA standards (0–500 μg/ml). Equal amounts of proteins were electrophoretically resolved on 12% SDS-PAGE and then transferred to Immunoblot PVDF membranes (Millipore). Membranes were cut to an appropriate size for loading controls with mouse anti-α-tubulin antibody (1:40,000, Sigma, Temecula, USA) and for target protein detection with rabbit anti-Rab18 antibody (1:500, Proteintech Group, USA). After washing, blots were incubated in horseradish-peroxidase-conjugated secondary antibodies (1:30,000, Sigma, USA). Proteins were visualized with Chemiluminescent HRP Substrate (Millipore). Images were captured on a Kodak Digital Science Image Station 440_{CF} and the band intensities were measured using Kodak Digital Science 1D, version 2.0.3.

Micro-magnetic resonance imaging

We followed the same protocol as Chen et al.'s (2011) to conduct the micro-magnetic resonance imaging (Micro-MRI) scanning. Briefly, 7-T scanner (PharmaScan 70/16, Bruker, Germany) was used for mouse brain analysis. All images from the longitudinal and cross-sectional experiments were processed using the manual tracing tool and edge editing function provided by ANALYZE (Biomedical Imaging Resource, Mayo Foundation, Rochester, Minnesota) (Chen et al., 2011).

Eye area and testis area measurements

We took the pictures of the evacuated eyes and testis with a ruler for volume quantifications. The eye and testis were outlined and the volume was calculated with the software Image-Pro Plus 5.0.

Beam walking

The apparatus used in this experiment was a modification of that used by Ferguson et al. (2010). Round beams (100 cm) with a diameter of 26 mm were used. The beam was covered with surgical tape that provided sufficient surface traction for the animals to walk on. The beam was suspended 60 cm above the floor. A black box was placed at the end of the beam as the finish point. Each mouse was given 2 consecutive trials and the average number of videotaped hind limb footslips was recorded. Slips were counted only while the mouse was in forward motion. The time to reach the black box was also recorded. A score of 5 indicated a flawless traverse; Score 4 indicated somewhat unsteady in traversing with no more than two footslips; Score 3 indicated over 2 but less than 10 footslips; Score 2 indicated over 10 footslips and a considerable amount of time traversing the beam; Score 1 indicated falling off before completing the walk; and Score 0 indicated immediate falling off.

Histological analysis

The lumbar spinal cords were isolated from *Rab18*$^{-/-}$, *Rab18*$^{+/+}$ and *Rab18*$^{-/-\text{Tg}Rab18\text{cDNA}}$ mice and then fixed immediately in formalin solution. Five-micrometer-thick paraffin sections of tissue cutting by a microtome were mounted on APS (Amino Silane) coated glass slides and heated at 55 °C for 30 min. Sections were cleared of paraffin in xylene and rehydrated through decreasing concentrations of ethanol. The HE stain and LFB were performed at the National Laboratory Animal Center, Taiwan.

Electron microscopy processing

The spinal cord, optic nerve and corpus callosum were immersed into a fixative solution containing 2.5% glutaraldehyde in 0.1 M phosphate buffer (pH 7.4) overnight. After washing in the same buffer, the tissues were postfixed in 1% OsO_4 for 2 h, dehydrated in a graded series of ethanol, infiltrated with propylene oxide/Spurr's resin and polymerized at 70 °C for 8 h. Semi-thin sections (0.5 μm thick) were prepared with an ultramicrotome (Leica Ultracut S), stained with Toluidine blue and observed and photographed on a Microscope (Olympus BX6). Ultrathin sections (60–70 nm thick) were obtained with an ultramicrotome (Leica Ultracut S), collected on copper grids, stained with uranyl acetate and lead citrate and observed and photographed on a JEM-2000EXII Transmission Electron Microscope.

Tests for pain and touch perceptions

Five to seven-month-old *Rab18*$^{-/-}$ mice and their littermate *Rab18*$^{+/+}$ and *Rab18*$^{-/-\text{Tg}Rab18\text{cDNA}}$ mice were used in the nociceptive tests. Thermal pain sensitivity was determined using hotplate or tail-flick methods (48, 50, or 52 °C). For the hotplate test, mice were placed on the incremental hot-plate analgesia meter (IITC Inc.) at 28 °C, and the plate temperature was increased to 55 °C with a computer-controlled rate of 6 °C/min. The latency (s) to show a nociceptive response with hind paw lick was recorded. The mouse was immediately removed when this response was observed. For tail-flick test, a radiant heat stimulus (SINGA Technology Corporation) was applied onto the mid-region of the tail and the intensity of the heat source was set at 50 or 52, which allowed the basal tail-flick latency to be controlled between before 20 s for all mice. The latency to tail flick was determined with a 30-s cutoff in 3 trials for each mouse and the mean was taken. The sensitivity to touch stimulation was applied to the middle plantar of each hind paw by placing the von Frey filament (Touch-Test kit, Stoelting) perpendicular to the surface of the paw. After a habituation period of 30 min, a series of six von Frey filaments (calibrated 0.008 g–0.4 g) was applied to one hind paw 5 times per trial. A positive response was defined as at least one clear paw withdrawal response out of the five applications. The response score was assessed as the total number of paw withdrawals in 10 trials for each filament and expressed as percentage (%).

Results

Rab18 mutant mouse model

We screened through 3126 male mice in 140 *N*-ethyl-*N*-nitrosourea (ENU)-mutagenized colonies using the open field test and direct behavioral observation. We found a mouse line in which 3 offspring displayed stomping gait (Fig. 1A) and abnormal clasping response (Fig. 1B). More mice with the same phenotype were identified when the colony was expanded, indicating that the phenotype could be inherited (Fig. S1). We initially mapped the mutation region with 40 microsatellite markers to chromosome 18. Further fine mapping and haplotype analysis using SNP genotyping with high-throughput MALDI-TOF mass spectrometry narrowed the mutation down to a 2.07 Mb region (Figs. 1C and S2). PCR and sequencing analyses identified a 7827-bp deletion spanning the promoter region, exon1, and a part of intron1 in the *Rab18* gene in the mutant mice (GenBank accession number JF701434) (Fig. 1D). No Rab18 protein was detected in the cerebellum of homozygous mutant mice. The heterozygotes expressed ~70% of Rab18 protein in the cerebellum in comparison with wild type (WT) mice (Fig. 1E).

Microphthalmia and microgenitalia in Rab18$^{-/-}$ *mice*

Since developmental abnormalities in the brain, eyes and reproductive system are the characteristic phenotypes of WARBM, we compared the brain, eyes and testis of *Rab18*$^{-/-}$ and WT mice. We used micro-MRI technique to evaluate the anatomical structure of the brain. There was no significant difference in the ventricle or total brain volume between *Rab18*$^{-/-}$ and WT mice (Fig. 2A and Table S1). The volume of the eyes in 10-month-old *Rab18*$^{-/-}$ mice ($N = 6$) was smaller than that of WT ($N = 4$) mice (16.2 ± 0.6 mm^3 versus 20.6 ± 0.6 mm^3, $P < 0.01$, Student's t-test) (Fig. 2B). The volume of testis in 10-month-old male *Rab18*$^{-/-}$ ($N = 6$) mice was also smaller than that of WT ($N = 4$) mice (588.3 ± 56.1 mm^3 versus 789.0 ± 56.7 mm^3, $P < 0.05$, Student's t-test) (Fig. 2C). The body weight of 2-month-old WT mice was obviously lower than that of 10-month-old WT mice (23.4 ± 1.3 g versus 32.0 ± 2.0 g, n = 7 per group, $P < 0.05$, Student's t-test), but their eye size (19.5 ± 0.8 mm^3 versus 20.6 ± 0.6 mm^3, n = 6 per group, $P = 0.28$, Student's t-test) and testis size (807.8 ± 40.6 mm^3 versus 789.0 ± 56.7 mm^3, n = 6 per group, $P = 0.80$, Student's t-test) were not significantly different. Therefore, smaller eye and testis size of *Rab18*$^{-/-}$ mice cannot be explained by lower body weight. These results indicate that microphthalmia and microgenitalia phenotypes found in WARBM patients were also exhibited in ENU-induced *Rab18* null mouse.

Stomping gait in Rab18$^{-/-}$ *mice*

Rab18$^{-/-}$ mice exhibited motor dysfunction, including improper limb placement and a stomping gait in the hind limbs (Fig. 1A). When *Rab18*$^{-/-}$ mice were two weeks old, they exhibited "waving tail" as well as excessive side to side movements in walking. The stomping gait became explicit when *Rab18*$^{-/-}$ mice were 5 months old; they lift their hind limbs high and hit the ground hard in walking (Fig. 1A and Video S1). This kind of gait is similar to that of the patients with sensory ataxia, who often slam their feet hard onto the ground in order to sense it. The symptom progressed and *Rab18*$^{-/-}$ mice developed a

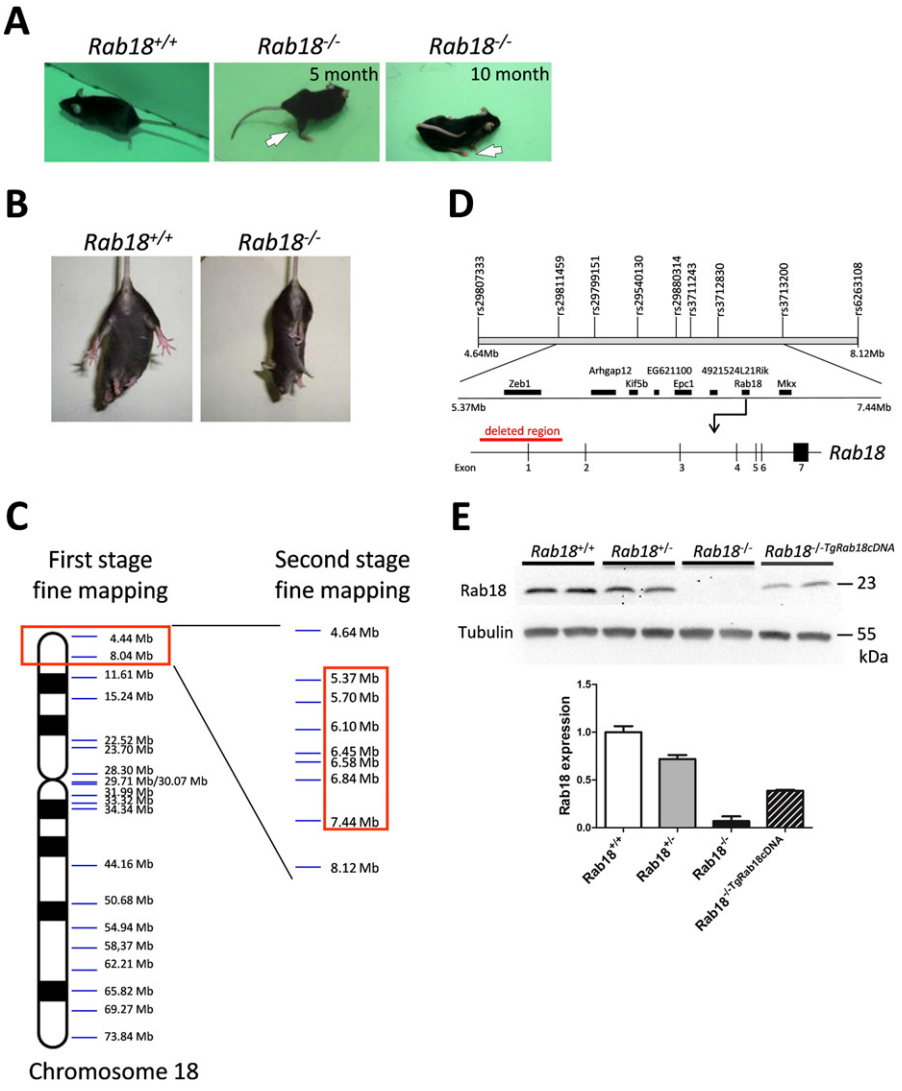

Fig. 1. The stomping phenotype in *Rab18*$^{-/-}$ mice was mapped to a large deletion in *Rab18*. (A) The 5-month stomping mouse (*Rab18*$^{-/-}$) lifted their feet higher than normal and stamped to ground in a violent manner in walking (arrow). The stomping mouse showed hind limb spasticity when they are 10 months old (arrow). (B) The 4-month stomping mouse (*Rab18*$^{-/-}$) clenched their hind limbs to the body, whereas the WT mice splayed their limbs and toes when suspended by the tail. (C) Two-stage fine mapping linkage analysis revealed that the mutation was located in the 5.37 Mb–7.44 Mb region on chromosome 18. (D) Eight candidate genes were predicted in this region. The markers used in the second-stage fine mapping were listed above. A 7827-bp deletion spanning the promoter, exon1, and a part of intron 1 of the *Rab18* gene was found by sequencing analysis in the stomping mice. (E) Western blot analysis of the Rab18 protein from the cerebellum. *Rab18*$^{-/-}$, *Rab18*$^{+/-}$, and *Rab18*$^{-/-\mathrm{Tg}Rab18\mathrm{cDNA}}$ mice expressed 7.0 ± 4.9%, 71.9 ± 4.3%, and 38.7 ± 1.0%, respectively (n = 2), of Rab18 protein relative to *Rab18*$^{+/+}$ mice.

spastic gait on the hind limbs when they were 10 months old (Fig. 1A and Video S2). When suspended by the tail, *Rab18*$^{-/-}$ mice retracted their hind limbs to the body and clenched their paws (Fig. 1B, right), while the legs of normal mice assumed a V position (Fig. 1B, left). The mean body weight of *Rab18*$^{-/-}$ mice was 12% lower than that of WT mice (Fig. S3). Nevertheless, *Rab18*$^{-/-}$ mice could survive longer than 15 months.

In order to confirm that those WARBM-like phenotypes were caused by the mutation of *Rab18* gene rather than by ENU-induced multiple mutations, we generated a rescued mouse line with an extra *Rab18* cDNA transgene in the *Rab18*$^{-/-}$ background. Pol II-driven *Rab18* Tg mice were crossed with *Rab18*$^{+/-}$ mice to produce *Rab18*$^{+/-}$ with $\mathrm{Tg}^{Rab18\mathrm{cDNA}}$ offspring which were then intercrossed to produce *Rab18*$^{-/-}$ with $\mathrm{Tg}^{Rab18\mathrm{cDNA}}$ (*Rab18*$^{-/-\mathrm{Tg}Rab18\mathrm{cDNA}}$) (Fig. S4). The Rab18 protein in the cerebellum of *Rab18*$^{-/-\mathrm{Tg}Rab18\mathrm{cDNA}}$ mice was 38.7 ± 1.0% compared to that of WT mice (Fig. 1E). The stomping gait of *Rab18*$^{-/-}$ mice was rescued by *Rab18* cDNA expression (Figs. 3A–C).

We used the beam walking test to evaluate *Rab18*$^{-/-}$ mice's motor function and balance (Fig. 3A). Impaired performance was noted since week 6 (Fig. 3B). Six-week-old *Rab18*$^{-/-}$ mice spent 10 s to walk through the 1.0-meter beam with occasional foot slippage (2.5 ± 1.1 times). At ages of four months and eight months, the number of foot slippage of *Rab18*$^{-/-}$ mice increased to 6.8 ± 2.2 and 9.0 ± 1.2 times, respectively. Twenty percent of 7-month *Rab18*$^{-/-}$ mice and 60% of 10-month *Rab18*$^{-/-}$ mice fell off the beam during the test (Fig. 3C). WT and *Rab18*$^{-/-\mathrm{Tg}Rab18\mathrm{cDNA}}$ mice walked normally without any foot slippage at all ages tested (Figs. 3A–C and Videos S3–S5). These results suggest that the stomping gait of *Rab18*$^{-/-}$ mice progresses with age.

Selective and progressive sensory axonal degeneration in Rab18$^{-/-}$ *mice*

In order to reveal the pathology of *Rab18*$^{-/-}$ mice's stomping gait, we performed pathological analysis in the nervous system of *Rab18*$^{-/-}$ mice. No significant morphological changes (data not shown) except for thinner corpus callosum in the brain sections stained

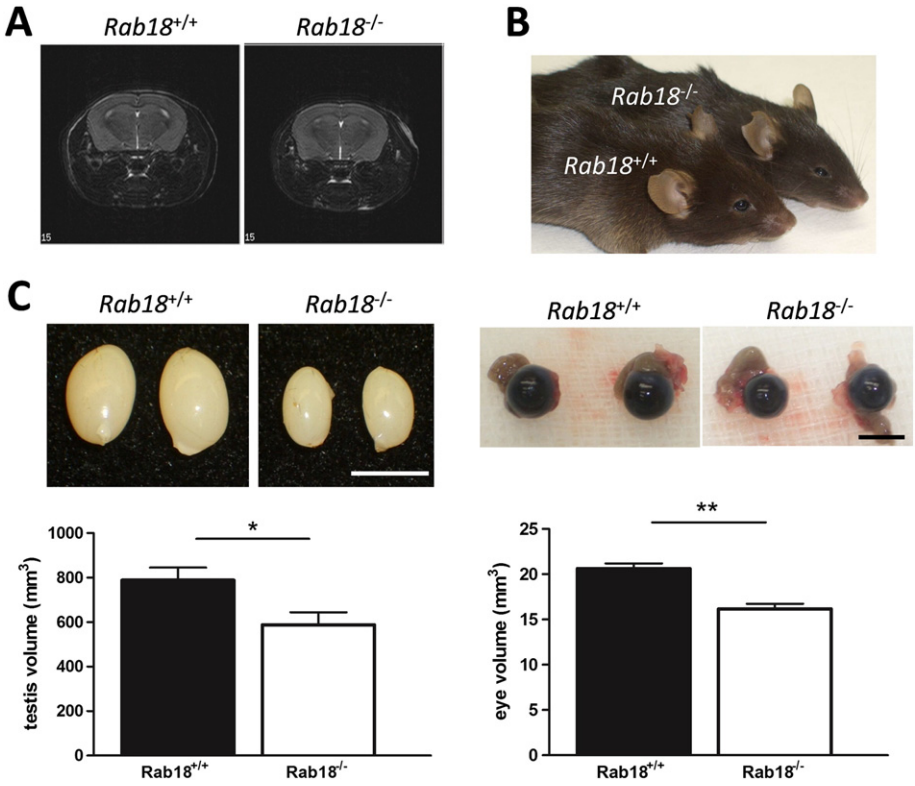

Fig. 2. Microphthalmia and microgenitalia in *Rab18*$^{-/-}$ mice. (A) Two in vivo obtained coronal 2D T2WI images of the head of a *Rab18*$^{-/-}$ mouse (right) and a WT mouse (left). Detailed volume analysis was summarized in Supplementary Table S1. (B) [Upper panel] Eye appearance of an adult *Rab18*$^{-/-}$ mouse (right) and a WT mouse (left). [Middle panel] The evacuated eyes of *Rab18*$^{-/-}$ mice were smaller than that of WT mice. Scale bar: 3 mm. [Lower panel] The eye volume of *Rab18*$^{-/-}$ mice was significantly smaller than that of WT mice. (C) [Upper panel] Photograph of the testes. The testis of *Rab18*$^{-/-}$ mice was smaller than that of WT mice. Scale bar: 5 mm. [Lower panel] The testis volume of *Rab18*$^{-/-}$ mice was significantly smaller than that of WT mice. *$P < 0.05$, **$P < 0.01$ vs. *Rab18*$^{-/-}$ group (Dunnett's post-hoc test following a one-way ANOVA).

with oil red O (Fig. S5A) were found in the brain. Spinal cord sections were stained with hematoxylin and eosin (HE) and Luxol fast blue (LFB) for pathological examinations. In HE stained sections, the dorsal column of *Rab18*$^{-/-}$ mice was obviously more restricted than that of *Rab18*$^{+/+}$ and *Rab18*$^{-/-\text{Tg}Rab18\text{cDNA}}$ mice (Fig. 3D). LFB stained sections showed an overall reduction without focal loss of LFB-positive area in the dorsal column, suggesting that axonal loss rather than myelination defect was randomly scattered throughout the stained area.

We further examined the semi-thin sections of the spinal cord and the dorsal roots of the lumbar spinal nerves with higher magnification. The gracile fasciculus and dorsal roots of *Rab18*$^{-/-}$ displayed several axons with signs of axonopathy. At 1.5 months, sporadic myelin dense bodies (Figs. 3E–F, the inset box) appeared in the gracile fasciculus and dorsal roots. More axons undergoing degenerating process were evident in the dorsal roots at 4 months. Less degenerated axons with increased non-axonal space at 8 months indicated significant axonal loss (Fig. 3F). To obtain a quantitative measure of the phenotype, we performed a morphological assessment for the axonopathy of the dorsal roots. *Rab18*$^{-/-}$ mice showed a significant increase in the number of degenerating axons as early as 1.5 months old (Fig. 3G). Although the dorsal roots exhibited obvious signs of degeneration, no obvious neuronal abnormality or loss was found in the dorsal root ganglion (DRG) of the *Rab18*$^{-/-}$ mice (Fig. S6). To determine whether sensory axons are selectively targeted for degeneration, we proceeded to examine the ventral roots of the spinal nerves in *Rab18*$^{-/-}$ mice. The ventral roots of the spinal nerves in *Rab18*$^{-/-}$ mice were intact and did not differ from those of WT mice in contrast to the dorsal roots of the spinal nerves in *Rab18*$^{-/-}$ mice (Fig. 4A). According to the pathological findings and the characteristic pattern of gait, we define *Rab18*$^{-/-}$ mice's stomping gait as a kind of sensory ataxia.

Because optic nerve degeneration is a characteristic phenotype of WARBM and the optic nerve is a cranial nerve (CN II) that sends special somatic afferent (sensory) fibers to the lateral geniculate of the thalamus, we also examined the optic nerves and found fibers undergoing degeneration with hyperdense axoplasm, watery swelling, and loosening myelin sheath (Fig. 4B).

Impaired perceptions of pain and touch in Rab18$^{-/-}$ *mice*

Since the sensory axons are selectively targeted for degeneration in *Rab18*$^{-/-}$ mice, we examined whether perceptions other than proprioception are affected (Fig. 4C). Thermal pain was evaluated by heat applied to the hind paws and high-intensity radiant heat applied to the tail. In the hot plate test, paw withdrawal latencies to heat were 201.8 ± 4.7 s (47.8 ± 0.5 °C) and 225.6 ± 4.9 s (50.2 ± 0.5 °C) for *Rab18*$^{+/+}$ and *Rab18*$^{-/-}$ mice, respectively (n = 5 per group, $P < 0.01$, Dunnett's post-hoc test). In the tail-flick test, *Rab18*$^{-/-}$ mice had a delayed response with a mean latency of 24.5 ± 1.8 s (intensity: 50) or 22.2 ± 1.6 s (intensity: 52), while WT mice had an average latency of 13.9 ± 1.6 s (intensity: 50) or 12.9 ± 1.6 s (intensity: 52) (n = 5 per group, $P < 0.01$, Dunnett's post-hoc test). The sensitivity to touch stimulation was assessed by response frequencies of paw withdrawal to the stimulation elicited by different forces of von Frey filaments. Application of a force of 0.4 g induced 100% of paw withdrawal response in WT mice but only ~1% of response was observed with the *Rab18*$^{-/-}$ mice. All the nociceptive responses in *Rab18*$^{-/-\text{Tg}Rab18\text{cDNA}}$ mice were similar to WT mice. The results indicated impaired perceptions of pain and touch in *Rab18*$^{-/-}$ mice.

Discussion

WARBM was found to be caused by germline mutations in *RAB3GAP1*, *RAB3GAP2*, *RAB18* and *TBC1D20*. These mutations cause indistinguishable ocular and neurological symptoms (Handley et al.,

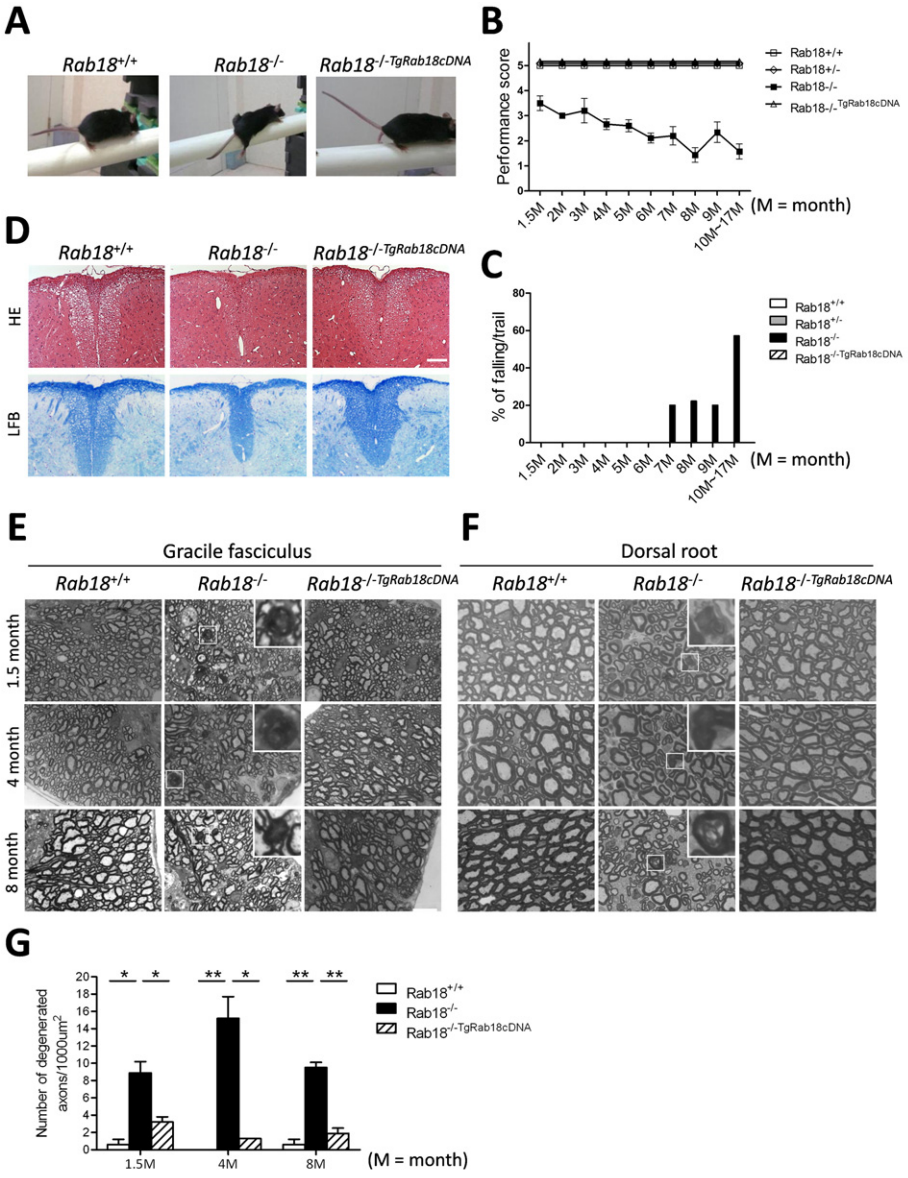

Fig. 3. Progressive stomping gait and axonal degeneration in *Rab18*$^{-/-}$ mice. Motor balance and coordination in mice were assessed using the beam walking test (A–C). (A) *Rab18*$^{+/+}$ and *Rab18*$^{-/-TgRab18cDNA}$ mice walked smoothly across the beam while *Rab18*$^{-/-}$ mice wobbled and repeatedly slipped in the test. (B) The performance score (1–5) of *Rab18*$^{-/-}$ mice decreased with age while *Rab18*$^{+/+}$, *Rab18*$^{+/-}$, and *Rab18*$^{-/-TgRab18cDNA}$ mice all have perfect score (n = 5 mice in each group). (C) *Rab18*$^{-/-}$ mice could walk on the beam without falling off the beam till 7 months old. The frequency of falling off increased with age. (D) [Upper panel] HE stain revealed marked atrophy in the posterior column of the lumbar spinal cord of *Rab18*$^{-/-}$ mice. [Lower panel] No evidence of demyelination was observed in the gracile fasciculus of *Rab18*$^{-/-}$ mice using LFB staining. Scale bar: 50 μm. (E and F) Semi-thin sections in the gracile fasciculus (E) and the dorsal root of the lumbar spinal nerves (F) were stained with Toluidine blue in different age groups. Multiple degenerated axons with collapsed myelin sheaths (myelin dense bodies) were seen in the *Rab18*$^{-/-}$ group. The inset showed a zoomed-in view of the box. Scale bar: 10 μm. (G) Quantification of axonal degeneration per 1000 μm^2 area in the dorsal root of the lumbar spinal nerves. Numbers of degenerated axons in *Rab18*$^{-/-}$ mice were all significantly higher than those in *Rab18*$^{+/+}$ and *Rab18*$^{-/-TgRab18cDNA}$ mice at three different ages (n = 2 mice in each group). $^{*}P < 0.05$, $^{**}P < 0.01$ vs. *Rab18*$^{-/-}$ group (Dunnett's post-hoc test following a one-way ANOVA).

2013; Bem et al., 2011; Liegel et al., 2013). It indicates that these four genes may share common signaling pathway and disease mechanism. In an attempt to determine the disease pathogenesis, mouse models for *Rab3gap1* and *TBC1D20* have been created, but fail to recapitulate the neurological and ocular features of WARBM (Liegel et al., 2013; Sakane et al., 2006). Recently, Carpanini et al. (2014) reported the characterization of a *Rab18*$^{-/-}$ mouse model that exhibited both the ocular and neurological features. This indicates that RAB18 may play an interactive or modulating role among the four causative genes in the neurological pathogenic mechanism of WARBM. Carpanini et al. (2014) also found that loss of Rab18 leads to widespread disruption of the neural cytoskeleton in peripheral nerve which provided the possible role of Rab18 into molecular mechanisms in disease pathogenesis. However, despite concerted effort, no any feature of neurodegeneration was observed in the nervous system. In this study, we demonstrate that loss of functional Rab18 leads to progressive sensory axonal degeneration and impairs responses to thermal pain and touch stimulation, which may contribute to the neurological deficits in patients with WARBM. Our findings narrow the gap between Carpanini et al.'s findings and the clinical/behavioral phenotypes in WARBM.

Normally, ENU introduced primarily point mutations rather than a deletion as large as ~7.8 kb in our ENU-induced *Rab18*$^{-/-}$ mice. Is it possible that our findings not found in Carpanini et al.'s *Rab18* knockout mice are caused by multiple mutations induced by ENU? The following three evidences support that the pathological and behavioral phenotypes observed in our ENU-induced *Rab18*$^{-/-}$ mice were exclusively caused by Rab18 loss-of-function. First, we had bred more than 15 generations and five hundred mice of this line, in which all the stomping

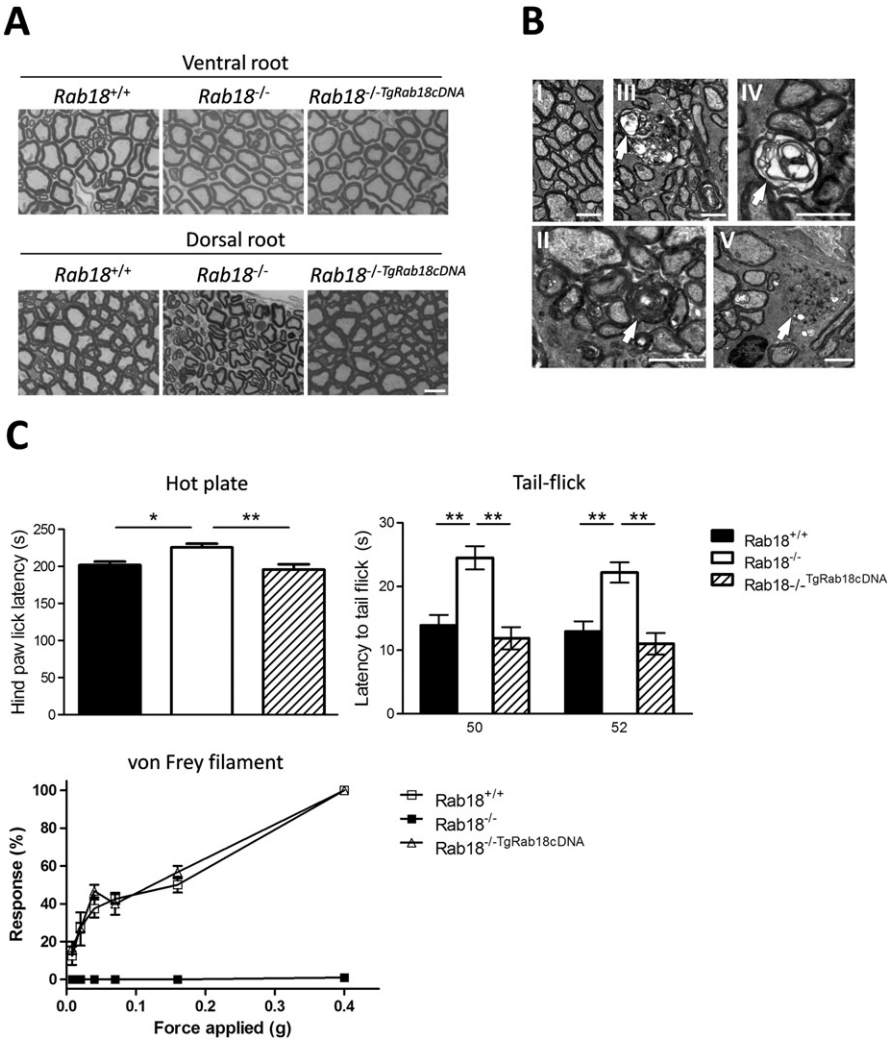

Fig. 4. Selective sensory axonal degeneration and impaired responses to thermal pain and mechanical stimulation in *Rab18*$^{-/-}$ mice. (A) Semi-thin sections of the ventral root of the lumbar spinal nerve stained with Toluidine blue. No degenerated axons were found in the ventral roots of the *Rab18*$^{-/-}$ mice, while the counterparts of the dorsal roots of the lumbar spinal nerves exhibited obvious signs of degeneration. Scale bar: 10 μm. (B) Electron micrographs of the optic nerves in (I) *Rab18*$^{+/+}$ and (II–V) *Rab18*$^{-/-}$ mice at 12 months old. The fibers in *Rab18*$^{+/+}$ mice were intact (I). In *Rab18*$^{-/-}$ mice, some fibers were undergoing degeneration with hyperdense axoplasm (arrow) (II), watery swelling (arrow) (III), and loosening myelin sheath (arrow) (IV). At the end stage of degeneration, more interstitial space with unrecognizable axonal structures and myelin debris (arrow) was left (V). Scale bar: 2 μm. (C) Responses to thermal pain and mechanical stimulation were measured by paw withdrawal latency in hot plate test and tail-flick latency. *Rab18*$^{-/-}$ mice displayed obviously longer response latencies in the hot-plate and tail-flick tests. Sensitivity to mechanical stimulation of *Rab18*$^{-/-}$ mice as measured by paw withdrawal threshold on expression to various forces of von Frey filaments was comparable to WT mice. Paw withdrawal responses in *Rab18*$^{-/-}$ were dramatically reduced. $^{*}P < 0.05$, $^{**}P < 0.01$ vs. *Rab18*$^{-/-}$ group (Dunnett's post-hoc test following a one-way ANOVA).

mice had homozygous *Rab18* deletion and all the heterozygous mice were normal in gait. Second, in a recent independent report by Carpanini et al., *Rab18* knockout mice by gene targeting exhibited similar phenotypes observed in our study (Carpanini et al., 2014). Finally, introducing an extra copy of the *Rab18* transgene could completely rescue the pathological and behavioral phenotypes observed in our ENU-induced *Rab18*$^{-/-}$ mice.

Children with WARBM do not learn to crawl or walk due to congenital hypotonia. They started to develop progressive spasticity on the lower limbs between 8 and 12 months old and on the upper limbs around 8 years old (Handley et al., 2013; Bem et al., 2011). Since spastic gait usually develops after a period of hypotonicity in the affected leg (Lippincott Williams and Wilkins, 2008), we tried to focus on the sign of hypotonia. Hypotonia can be caused by deficits in the muscles or within the central nervous system. We examined the quadriceps femoris and gluteal muscles of *Rab18*$^{-/-}$ mice with HE, ATPase and NADH-TR stains. All the examinations did not find specific pathology except some sporadic fibrosis (data not shown). Therefore, the hypotonia is most likely due to some kind of pathology in the central nervous system, which disrupts the complex feedback loops of sensory processing and motor output. If an animal's sensory processing (vestibular, proprioceptive and tactile) is jeopardized, its brain cannot receive the messages of changes in body position, and then it may exhibit a stomping gait to confirm the hits of its feet on the ground. Our pathological and behavioral findings support that hind limbs weakness in *Rab18*$^{-/-}$ mice may be influenced by sensory impairment. However, incoordination due to sensory ataxia can mimic cerebellar ataxia (Campbell and DeJong, 2013) and patients with WARBM have cerebellar vermis hypoplasia, we examined the cerebellum and found Purkinje cell loss in 9 M *Rab18*$^{-/-}$ mice (data not shown). Since ataxia gait precedes Purkinje cell loss for almost seven months and most of the vermal and paravermal regions of the cerebellum receive extensive somatosensory input from the spinal cord (Fredericks and Saladin, 1996), the cerebellar pathology probably reflects the loss of cerebellar afferents. The neurological pathology is similar to that of Friedreich's ataxia which may have some patchy loss of cerebellar Purkinje cells and mild degenerative changes in cerebellar nuclei, but the ataxia of movement is largely a result of the loss of proprioceptive sense (Fredericks and Saladin,

1996; Wells et al., 2006). In addition, the beam walking test indicated that gait abnormality started around 1.5 months old when sensory axonal neuropathy was noted in pathological examination. Taken together, axonal degeneration in the sensory roots and dorsal column of the spinal cord is the primary cause of sensory ataxia in *Rab18*$^{-/-}$ mice.

Patients with WARBM also suffer from progressive visual loss. Their poor vision is initially due to congenital cataracts, but their vision keeps on deteriorating even after lens replacement surgery. Electroretinogram (ERG) revealed that the patient had progressive optic atrophy and impairment in the visual cortex (Bem et al., 2011). In our study, we found obvious axonal degeneration in the optic nerves of *Rab18*$^{-/-}$ mice. Our findings clarify the underlying cause of progressive deterioration in clinical and electrophysiological findings in WARBM children's vision.

Axonal degenerations in the optic nerve and the sensory roots of the spinal nerves with intact motor roots indicate that Rab18 has a specific role in the sensory nervous system. Rab proteins have long been known to be involved in vesicle transport processes in different cell types. Due to the complexity of axons and dendrites of neurons, vesicle transport is an important process to maintain synaptic functions and axonal connectivity by transporting molecules along the neurites. Therefore the nervous system is especially vulnerable to defects in vesicle transport (Millecamps and Julien, 2013; Morfini et al., 2009; De Vos et al., 2008). Carpanini et al. recently found that loss of Rab18 was associated with widespread disruption of the neuronal cytoskeleton, including abnormal accumulations of neurofilament and microtubule proteins in synaptic terminals, and gross disorganization of the cytoskeleton in peripheral nerves (Carpanini et al., 2014). Abnormal neurofilament accumulation is a common toxic intermediate and is a prominent cytopathology feature in several neurodegenerative diseases (Goldman and Yen, 1986; Pollanen et al., 1993; Lee and Cleveland, 1994). In addition, reduced expression and delivery of neurofilament subunits to the distal axon has been proposed as a critical factor in the etiology of sensory axonal degeneration (Scott et al., 1999; Fernyhough et al., 1999; Fernyhough and Schmidt, 2002). More recently, Gerondopoulos et al. suggested that Rab18 activity was important for ER structure because ER tubular networks were disrupted and ER sheets spread out into the cell periphery in the absence of Rab18 (Gerondopoulos et al., 2014). Alterations in the architecture of the ER might induce ER stress which has been implicated in retrograde neuronal degeneration (Lindholm et al., 2006; Doyle et al., 2011). In addition, ER represents an important Ca^{2+} storage organelle in DRG sensory neurons (Solovyova et al., 2002) and RAB18 was reported to regulate Ca^{2+}-mediated exocytosis in neuroendocrine cell (Vazquez-Martinez et al., 2007). Abnormal neuronal Ca^{2+} homeostasis has been implicated in numerous CNS and PNS diseases including diabetic sensory neuropathy (Verkhratsky and Fernyhough, 2008). Whether neurofilament accumulation or defective ER function is the primary reason of sensory axonal degeneration in *Rab18*$^{-/-}$ mice requires further clarification.

Since axonal degeneration was presented in the optic nerves and sensory roots of the spinal nerves of *Rab18*$^{-/-}$ mice, loss of Rab18 may attribute to general deficiency of sensory inputs. Sensory inputs are necessary for brain functioning and promote development in all areas. After birth, sensory experiences modulate cortical development, inducing both functional and anatomical cortical architecture (Greenough et al., 1987; Katz and Shatz, 1996; Hensch, 2004). In humans, loss of functional RAB18 protein leads to microcephaly, hypogenesis of the corpus callosum and profound mental retardation. Our *Rab18*$^{-/-}$ mice also have the phenotypes of thinner corpus callosum (Fig. S4A), but no evidence of axonal degeneration could be found therein (Fig. S4B), suggesting that hypoplastic corpus callosum is due to defective neurodevelopment rather than neurodegeneration. Our findings indicate that Rab18 deficiency results in neurodevelopmental and neurodegenerative problems in different parts of the nervous system. However, *Rab18*$^{-/-}$ mice do not have the characteristic phenotypes of microcephaly and mental retardation of WARBM. Our *Rab18*$^{-/-}$ mice performed as well as WT mice in the freezing test and multiple T-maze test (data not shown). This implicates that Rab18 may have an important role in the development of cerebral cortex which shares a substantially larger proportion of the brain in humans and animals with higher intelligence. Interestingly, deficits in sensory processing are common in certain mental disorders such as schizophrenia (Ross et al., 2007; Butler et al., 2001; Foxe et al., 2001; Javitt et al., 1999; Adler et al., 1998; Sanchez-Morla et al., 2008). Using a translational convergent functional genomics approach, Ayalew et al. reported that *RAB18* was an important candidate gene of schizophrenia (Ayalew et al., 2012).

In summary, our results reveal that sensory axonal degeneration is the primary cause of stomping gait and progressive weakness of the hind limbs in *Rab18*$^{-/-}$ mice, and optic nerve degeneration should be the major pathology of progressive optic atrophy in children with WARBM. Our results indicate that the sensory nervous system is more vulnerable to Rab18 deficiency and WARBM is not simply a developmental disease but also a neurodegenerative disease.

Supplementary data to this article can be found online at http://dx.doi.org/10.1016/j.expneurol.2015.03.003.

Funding

This work was supported by grants from the National Science Council Taiwan (NSC 102-2314-B-075-005-MY3), the Taipei Veterans General Hospital (V103E9-004 and V102C-173), and the Ministry of Education Taiwan, Aim for the Top University Plan (104AC-B6).

Author contributions

C.J.H. and C.Y.C. approached and designed the project. C.Y.C. and P.C.W. performed the experiments. C.J.H., C.Y.C., J.C.W., S.J.T. and Y.J.L. provided the concept of the paper. C.J.H., C.Y.C., J.W.T., L.S.K. and M.J.F. interpreted the data being published. C.J.H., C.Y.C., J.W.T. and F.S.N. wrote the paper. C.J.H. and C.Y.T. edited the article.

Conflict of interest

The authors declare no conflict of interest.

Acknowledgment

The authors thank the Taiwan National Mouse Mutagenesis Program Core Facility for providing ENU-mutagenized mice; Mr. Chuan-Kai Chou (National Laboratory Animal Center, Taiwan) for cryopreservation; Dr. Pang-Hsien Tu (Institute of Biomedical Sciences, Academia Sinica, Taipei, Taiwan), Dr. Ko-Pei Kao (Department of Neurology, Neurological Institute, Taipei Veterans General Hospital), Dr. Kon-Ping Lin (Department of Neurology, Neurological Institute, Taipei Veterans General Hospital), Dr. Shuu-Jiun Wang (Department of Neurology, Neurological Institute, Taipei Veterans General Hospital), Dr. An-Hang Yang (Division of Ultrastructural and Molecular Pathology, Department of Pathology, Taipei Veterans General Hospital) and Division of Experimental Surgery of the Department of Surgery (Taipei Veterans General Hospital) for technical supports and discussions on pathological examinations; National Center for Genome Medicine for gene mapping; Dr. Ting-Fen Tsai (Department of Life Sciences and institute of Genome Sciences, National Yang-Ming University) for providing pol II–IVS vector and consultation in the generation of *Rab18* transgenic mice; Animal Behavioral Core at Brain Research Center (National Yang-Ming University) for behavior studies; Functional and Micro-Magnetic Resonance Imaging Center (Academia Sinica, Taipei, Taiwan) for MRI technical support; Taiwan Mouse Clinic (Academia Sinica, Taipei, Taiwan) for technical support for HE and LFB stains.

References

Abdel-Salam, G.M., Hassan, N.A., Kayed, H.F., Aligianis, I.A., 2007. Phenotypic variability in Micro syndrome: report of new cases. Genet. Couns. 18, 423–435.

Adler, L.E., Olincy, A., Waldo, M., Harris, J.G., Griffith, J., et al., 1998. Schizophrenia, sensory gating, and nicotinic receptors. Schizophr. Bull. 24, 189–202.

Aligianis, I.A., Johnson, C.A., Gissen, P., Chen, D., Hampshire, D., et al., 2005. Mutations of the catalytic subunit of RAB3GAP cause Warburg Micro syndrome. Nat. Genet. 37, 221–223.

Ayalew, M., Le-Niculescu, H., Levey, D.F., Jain, N., Changala, B., et al., 2012. Convergent functional genomics of schizophrenia: from comprehensive understanding to genetic risk prediction. Mol. Psychiatry 17, 887–905.

Balling, R., 2001. ENU mutagenesis: analyzing gene function in mice. Annu. Rev. Genomics Hum. Genet. 2, 463–492.

Bem, D., Yoshimura, S., Nunes-Bastos, R., Bond, F.C., Kurian, M.A., et al., 2011. Loss-of-function mutations in RAB18 cause Warburg micro syndrome. Am. J. Hum. Genet. 88, 499–507.

Borck, G., Wunram, H., Steiert, A., Volk, A.E., Korber, F., et al., 2011. A homozygous RAB3GAP2 mutation causes Warburg Micro syndrome. Hum. Genet. 129, 45–50.

Butler, P.D., Schechter, I., Zemon, V., Schwartz, S.G., Greenstein, V.C., et al., 2001. Dysfunction of early-stage visual processing in schizophrenia. Am. J. Psychiatry 158, 1126–1133.

Campbell, W.W., DeJong, R.N., 2013. DeJong's the Neurologic Examination/William W. Campbell. xii. Lippincott Williams & Wilkins, Philadelphia, PA (819 p. p.).

Carpanini, S.M., McKie, L., Thomson, D., Wright, A.K., Gordon, S.L., et al., 2014. A novel mouse model of Warburg Micro syndrome reveals roles for RAB18 in eye development and organisation of the neuronal cytoskeleton. Dis. Model. Mech. 7, 711–722.

Chen, C.C., Tung, Y.Y., Chang, C., 2011. A lifespan MRI evaluation of ventricular enlargement in normal aging mice. Neurobiol. Aging 32, 2299–2307.

Corbeel, L., Freson, K., 2008. Rab proteins and Rab-associated proteins: major actors in the mechanism of protein-trafficking disorders. Eur. J. Pediatr. 167, 723–729.

De Vos, K.J., Grierson, A.J., Ackerley, S., Miller, C.C., 2008. Role of axonal transport in neurodegenerative diseases. Annu. Rev. Neurosci. 31, 151–173.

Derbent, M., Agras, P.I., Gedik, S., Oto, S., Alehan, F., et al., 2004. Congenital cataract, microphthalmia, hypoplasia of corpus callosum and hypogenitalism: report and review of Micro syndrome. Am. J. Med. Genet. A 128A, 232–234.

Doyle, K.M., Kennedy, D., Gorman, A.M., Gupta, S., Healy, S.J., et al., 2011. Unfolded proteins and endoplasmic reticulum stress in neurodegenerative disorders. J. Cell. Mol. Med. 15, 2025–2039.

Ferguson, M.C., Nayyar, T., Deutch, A.Y., Ansah, T.A., 2010. 5-HT2A receptor antagonists improve motor impairments in the MPTP mouse model of Parkinson's disease. Neuropharmacology 59, 31–36.

Fernyhough, P., Schmidt, R.E., 2002. Neurofilaments in diabetic neuropathy. Int. Rev. Neurobiol. 50, 115–144.

Fernyhough, P., Gallagher, A., Averill, S.A., Priestley, J.V., Hounsom, L., et al., 1999. Aberrant neurofilament phosphorylation in sensory neurons of rats with diabetic neuropathy. Diabetes 48, 881–889.

Foxe, J.J., Doniger, G.M., Javitt, D.C., 2001. Early visual processing deficits in schizophrenia: impaired P1 generation revealed by high-density electrical mapping. Neuroreport 12, 3815–3820.

Fredericks, C.M., Saladin, L.K., 1996. Pathophysiology of the Motor Systems: Principles and Clinical Presentations. xxvii. F.A. Davis, Philadelphia (594 p. p.).

Gerondopoulos, A., Bastos, R.N., Yoshimura, S., Anderson, R., Carpanini, S., et al., 2014. Rab18 and a Rab18 GEF complex are required for normal ER structure. J. Cell Biol. 205, 707–720.

Goldman, J.E., Yen, S.H., 1986. Cytoskeletal protein abnormalities in neurodegenerative diseases. Ann. Neurol. 19, 209–223.

Goody, R.S., Rak, A., Alexandrov, K., 2005. The structural and mechanistic basis for recycling of Rab proteins between membrane compartments. Cell. Mol. Life Sci. 62, 1657–1670.

Greenough, W.T., Black, J.E., Wallace, C.S., 1987. Experience and brain development. Child Dev. 58, 539–559.

Haas, A.K., Yoshimura, S., Stephens, D.J., Preisinger, C., Fuchs, E., et al., 2007. Analysis of GTPase-activating proteins: Rab1 and Rab43 are key Rabs required to maintain a functional Golgi complex in human cells. J. Cell Sci. 120, 2997–3010.

Handley, M.T., Morris-Rosendahl, D.J., Brown, S., Macdonald, F., Hardy, C., et al., 2013. Mutation spectrum in RAB3GAP1, RAB3GAP2, and RAB18 and genotype–phenotype correlations in Warburg micro syndrome and Martsolf syndrome. Hum. Mutat. 34, 686–696.

Hensch, T.K., 2004. Critical period regulation. Annu. Rev. Neurosci. 27, 549–579.

Hrabe de Angelis, M.H., Flaswinkel, H., Fuchs, H., Rathkolb, B., Soewarto, D., et al., 2000. Genome-wide, large-scale production of mutant mice by ENU mutagenesis. Nat. Genet. 25, 444–447.

Javitt, D.C., Liederman, E., Cienfuegos, A., Shelley, A.M., 1999. Panmodal processing imprecision as a basis for dysfunction of transient memory storage systems in schizophrenia. Schizophr. Bull. 25, 763–775.

Jurinke, C., van den Boom, D., Cantor, C.R., Koster, H., 2002. The use of MassARRAY technology for high throughput genotyping. Adv. Biochem. Eng. Biotechnol. 77, 57–74.

Justice, M.J., 2000. Capitalizing on large-scale mouse mutagenesis screens. Nat. Rev. Genet. 1, 109–115.

Katz, L.C., Shatz, C.J., 1996. Synaptic activity and the construction of cortical circuits. Science 274, 1133–1138.

Lee, M.K., Cleveland, D.W., 1994. Neurofilament function and dysfunction: involvement in axonal growth and neuronal disease. Curr. Opin. Cell Biol. 6, 34–40.

Liegel, R.P., Handley, M.T., Ronchetti, A., Brown, S., Langemeyer, L., et al., 2013. Loss-of-function mutations in TBC1D20 cause cataracts and male infertility in blind sterile mice and Warburg micro syndrome in humans. Am. J. Hum. Genet. 93, 1001–1014.

Lindholm, D., Wootz, H., Korhonen, L., 2006. ER stress and neurodegenerative diseases. Cell Death Differ. 13, 385–392.

Lippincott Williams & Wilkins, 2008. Portable Signs & Symptoms. iv. Wolters Kluwer/Lippincott Williams & Wilkins, Philadelphia (604 p. p.).

Millecamps, S., Julien, J.P., 2013. Axonal transport deficits and neurodegenerative diseases. Nat. Rev. Neurosci. 14, 161–176.

Morfini, G.A., Burns, M., Binder, L.I., Kanaan, N.M., LaPointe, N., et al., 2009. Axonal transport defects in neurodegenerative diseases. J. Neurosci. 29, 12776–12786.

Neuhaus, I.M., Beier, D.R., 1998. Efficient localization of mutations by interval haplotype analysis. Mamm. Genome 9, 150–154.

Pollanen, M.S., Dickson, D.W., Bergeron, C., 1993. Pathology and biology of the Lewy body. J. Neuropathol. Exp. Neurol. 52, 183–191.

Ross, L.A., Saint-Amour, D., Leavitt, V.M., Molholm, S., Javitt, D.C., et al., 2007. Impaired multisensory processing in schizophrenia: deficits in the visual enhancement of speech comprehension under noisy environmental conditions. Schizophr. Res. 97, 173–183.

Sakane, A., Manabe, S., Ishizaki, H., Tanaka-Okamoto, M., Kiyokage, E., et al., 2006. Rab3 GTPase-activating protein regulates synaptic transmission and plasticity through the inactivation of Rab3. Proc. Natl. Acad. Sci. U. S. A. 103, 10029–10034.

Sanchez-Morla, E.M., Garcia-Jimenez, M.A., Barabash, A., Martinez-Vizcaino, V., Mena, J., et al., 2008. P50 sensory gating deficit is a common marker of vulnerability to bipolar disorder and schizophrenia. Acta Psychiatr. Scand. 117, 313–318.

Scott, J.N., Clark, A.W., Zochodne, D.W., 1999. Neurofilament and tubulin gene expression in progressive experimental diabetes: failure of synthesis and export by sensory neurons. Brain 122 (Pt 11), 2109–2118.

Sklan, E.H., Serrano, R.L., Einav, S., Pfeffer, S.R., Lambright, D.G., et al., 2007. TBC1D20 is a Rab1 GTPase-activating protein that mediates hepatitis C virus replication. J. Biol. Chem. 282, 36354–36361.

Solovyova, N., Veselovsky, N., Toescu, E.C., Verkhratsky, A., 2002. Ca(2+) dynamics in the lumen of the endoplasmic reticulum in sensory neurons: direct visualization of Ca(2+)-induced Ca(2+) release triggered by physiological Ca(2+) entry. EMBO J. 21, 622–630.

Stenmark, H., Olkkonen, V.M., 2001. The Rab GTPase family. Genome Biol. 2 (REVIEWS3007).

Takai, Y., Sasaki, T., Matozaki, T., 2001. Small GTP-binding proteins. Physiol. Rev. 81, 153–208.

Vazquez-Martinez, R., Cruz-Garcia, D., Duran-Prado, M., Peinado, J.R., Castano, J.P., et al., 2007. Rab18 inhibits secretory activity in neuroendocrine cells by interacting with secretory granules. Traffic 8, 867–882.

Verkhratsky, A., Fernyhough, P., 2008. Mitochondrial malfunction and Ca2+ dyshomeostasis drive neuronal pathology in diabetes. Cell Calcium 44, 112–122.

Warburg, M., Sjo, O., Fledelius, H.C., Pedersen, S.A., 1993. Autosomal recessive microcephaly, microcornea, congenital cataract, mental retardation, optic atrophy, and hypogenitalism. Micro syndrome. Am. J. Dis. Child. 147, 1309–1312.

Weber, J.S., Salinger, A., Justice, M.J., 2000. Optimal N-ethyl-N-nitrosourea (ENU) doses for inbred mouse strains. Genesis 26, 230–233.

Wells, R.D., Warren, S.T., Sarmiento, M., 2006. Genetic Instabilities and Neurological Diseases. xv. Elsevier, Amsterdam; Boston (766 p. p.).